Carbon Nanotubes as a Framework for High-Aspect-Ratio MEMS Fabrication

David N. Hutchison, Nicholas B. Morrill, Quentin Aten, Brendan W. Turner, Brian D. Jensen, Larry L. Howell, *Fellow, ASME*, Richard R. Vanfleet, and Robert C. Davis

***Abstract*—A class of carbon-nanotube (CNT) composite materials was developed to take advantage of the precise high-aspect-ratio shape of patterned vertically grown nanotube forests. These patterned forests were rendered mechanically robust by chemical vapor infiltration and released by etching an underlying sacrificial layer. We fabricated a diverse variety of functional MEMS devices, including cantilevers, bistable mechanisms, and thermomechanical actuators, using this technique. A wide range of chemical-vapor-depositable materials could be used as fillers; here, we specifically explored infiltration by silicon and silicon nitride. The CNT framework technique may enable high-aspect-ratio MEMS fabrication from a variety of materials with desired properties such as high-temperature stability or robustness. The elastic modulus of the silicon-nanotube and silicon nitride-nanotube composites is dominated by the filler material, but they remain electrically conductive, even when the filler (over 99% of the composite's mass) is insulating. [2009-0197]**

***Index Terms*—Carbon, fabrication, microelectromechanical devices, nanotechnology.**

I. Introduction and Process Overview

HIGH-ASPECT-RATIO geometries are often desirable in MEMS for increased mechanical robustness, reduced out-of-plane motion of flexures, and increased surface area for functionalization or capacitive actuation and detection [2]. Consequently, considerable effort has been invested in developing various high-aspect-ratio fabrication methods. Deep reactive ion etching (DRIE) has become a standard method of deep etching silicon, and LIGA is another method that may be used to attain even higher aspect ratios. We demonstrate a CNT-framework-based approach to high-aspect-ratio MEMS fabrication and find that it has some significant potential advantages over DRIE- and LIGA-based techniques.

Manuscript received May 7, 2009; revised September 8, 2009. First published December 8, 2009; current version published February 3, 2010. Subject Editor G. K. Fedder.

D. N. Hutchison was with the Department of Physics and Astronomy, Brigham Young University, Provo, UT 84602 USA. He is now with the School of Applied and Engineering Physics, Cornell University, Ithaca, NY 14853 USA.

N. B. Morrill, R. R. Vanfleet, and R. C. Davis are with the Department of Physics and Astronomy, Brigham Young University, Provo, UT 84602 USA (e-mail: davis@byu.edu).

Q. Aten, B. D. Jensen, and L. L. Howell are with the Department of Mechanical Engineering, Brigham Young University, Provo, UT 84602 USA.

B. W. Turner was with the Department of Physics and Astronomy, Brigham Young University, Provo, UT 84062 USA. He is now with the Graduate Group in Applied Science and Technology, University of California at Berkeley, Berkeley, CA 94720 USA.

Color versions of one or more of the figures in this paper are available online at http://ieeexplore.ieee.org.

Digital Object Identifier 10.1109/JMEMS.2009.2035639

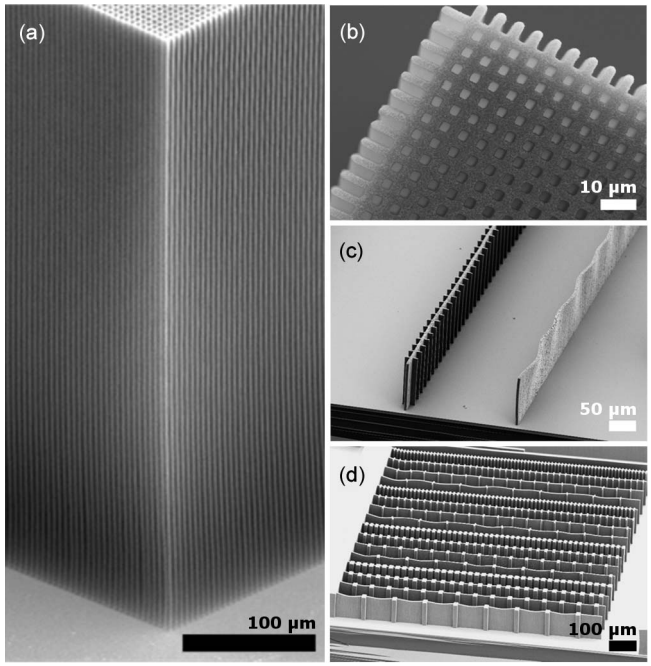

Fig. 1. Extreme aspect-ratio patterned nanotube growth and self-supporting architectures. (a) Tilted view and (b) top view of a pattern of 3-μm square holes, grown 580 μm tall. (c) Self-supporting architectures allow free-standing nanotube patterns to grow vertically to much higher aspect ratios. The crossbar architecture shown allows the 5-μm-wide line on the left to reliably grow up to four times taller than the same width line on the right, without bending. These nanotube forests have been filled with silicon. Imaged at 50° tilt. (d) Several 1-mm-long 5-μm-wide lines grown to a height of about 100 μm, with various crossbar widths and spacings. Widely spaced crossbars do little to help the lines grow straight (evident in this image as a "waviness" on the top of these lines), but more closely spaced crossbars support the nanotube structure while preserving the high compliance of thin beams such as these. Imaged at 50° tilt.

Our approach consists of using the extraordinarily high aspect ratios of vertically aligned carbon-nanotube (VACNT) structures (Fig. 1) as a mechanical framework for high-aspect-ratio MEMS fabrication. After growing a framework of VACNTs from a patterned catalyst film, the framework is infiltrated with a "filler" material by low-pressure chemical vapor deposition (LPCVD), as shown in Fig. 2. Because the unfilled forest has very low density (about 0.009 g/cm^3 in air, or only 7.5 times the mass of the same volume of air), the filled forest consists mostly of the filler. The filling step also deposits a "floor layer" of the filler material in regions where there are no nanotubes, indicated by the black oval in Fig. 2(c). A short reactive ion etch (RIE) was used to remove the floor layer. The active parts of the MEMS structures are then

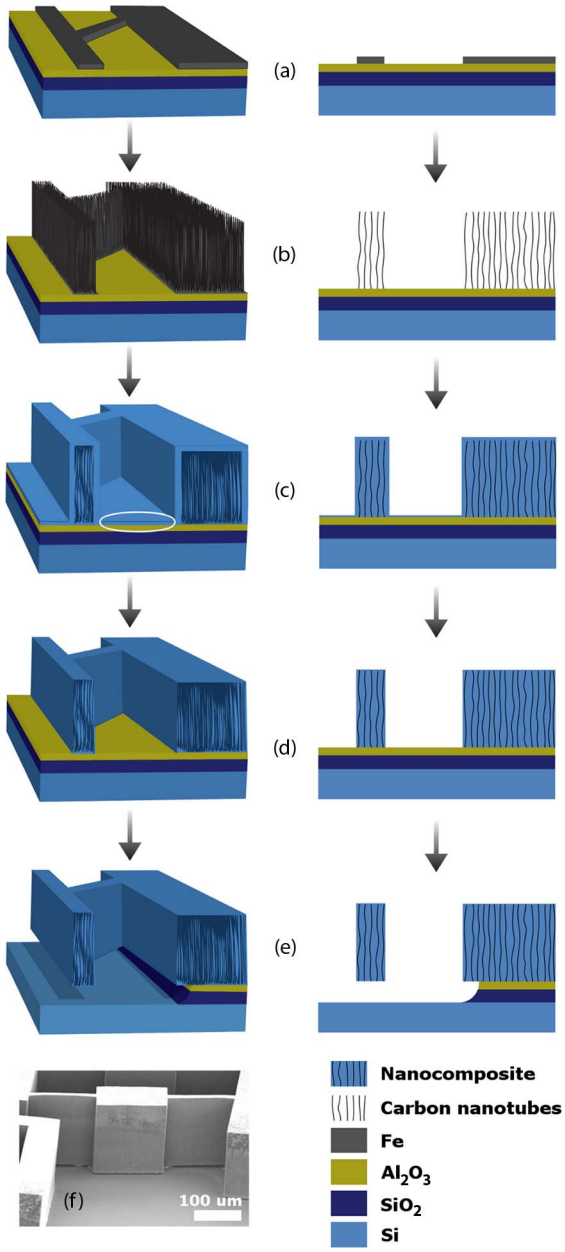

Fig. 2. Process diagram. (a) Fe film of 4 nm is thermally evaporated and lithographically patterned by liftoff on 20 nm of e-beam-evaporated Al_2O_3 on 3-μm PECVD SiO_2 on Si. The Fe is a catalyst for subsequent VACNT growth. Al_2O_3 is a solid diffusion barrier to prevent the iron catalyst from forming iron silicide at CNT growth temperature. SiO_2 is a sacrificial layer for later release. (b) Vertically aligned nanotubes are grown from the Fe film. (c) Interstices between tubes are filled with silicon, silicon nitride, or other materials by LPCVD. This not only fills the forest but also deposits a "floor layer," indicated by a white oval. (d) Floor layer is much thinner than the filled forests, so it may be removed by RIE without removing the bulk of the nanocomposite. (e) Underlying SiO_2 layer is removed by immersion in buffered HF. (f) SEM image showing part of a MEMS device corresponding to step (e).

released by wet etching an underlying sacrificial layer. The final structure is an extremely high aspect-ratio MEMS device made from a patterned nanocomposite material. The nanocomposite consists of a "filler" material (we used undoped polysilicon and silicon nitride) and an aligned "framework" of nanotubes. Our nanocomposites exhibited mechanical properties dominated by the filler material but electrical conductivity due primarily to the VACNT framework.

We have filled the nanotube forests with LPCVD from single-source and dual-source precursors, but other interesting CVD filler materials include ceramics, metals, and polymers. Most elements in the periodic table were deposited by CVD in the past [3], either in elemental form or in combinations with other elements. This variety of materials can enable a wide range of applications requiring high-temperature stability, high stiffness, strength, biocompatibility, or a host of other mechanical, electrical, and chemical properties. Thus, the nanotube framework technique may enable fabrication of 3-D structures with this broad palette of materials, even when the materials cannot be effectively etched vertically. Additionally, the LPCVD infiltration step takes advantage of the large internal surface area of the nanotube forest to make large solid structures tens or hundreds of micrometers tall by depositing less than 300 nm of the filler material, just enough to fill the interstices between tubes. Therefore, this technique may naturally extend to fillers that are slow or expensive to deposit by CVD.

As-grown VACNT structures are only very weakly held together due to their low density and weak intertube van der Waals bonding. Methods that have been employed to increase the cohesiveness of VACNT forests include the use of capillary forces to densify the forests [4], [5], as well as infiltration of the forests with a filler to form a composite. Composite fillers include polymers [6]–[9], diamondlike carbon [10], copper [11], silica [12], silicon, and silicon nitride [13]. Micromechanical devices have been fabricated from both densified VACNTs [5], [14] and infiltrated VACNTs [7], [8]. Specifically, Hayamizu *et al.* used densified "CNT wafers" to fabricate electrically actuated switches and singly and doubly clamped beams [5]. Fang *et al.* found that patterned CNT forests filled with CVD-deposited parylene display a nanoindentation hardness that is 14 times that of unfilled forests, and made and tested aligned CNT-parylene singly and doubly clamped beams [7], [8]. However none of the previous work exploits the possibility of using highly vertical patterned CNT growth to fabricate functioning high-aspect-ratio MEMS.

We demonstrate a diverse range of functioning high-aspect-ratio microelectromechanical devices (aspect ratios of hundreds-to-one) using much harder materials (silicon and silicon nitride). We perform electrical resistivity measurements and test the in-plane flexural bending of aligned CNT-composite cantilevers. We demonstrate extremely vertical sidewalls and flat forest tops and show the importance of vapor access holes and self-supporting architectures in achieving extremely high aspect-ratio microstructures. Our devices do not also exhibit signs of curl-up associated with residual stress.

This technique has some attractive features when compared to DRIE. DRIE is, in most cases, limited to silicon, whereas the present technique can be applied to many CVD-depositable materials. The CNT growth rate is very high (40–60 μm/min for the first few minutes) compared to DRIE rates (about 10 μm/min or less), favoring high industrial throughput, and the sidewall roughness is comparable to that obtained by DRIE processes. These advantages are compounded by the inherent scalability of CVD processes, compared to the serial nature of DRIE processing. LIGA is another technique that allows for extreme aspect-ratio fabrication with some of these materials

(specifically electroformable metals and polymers) but requires a synchrotron facility [15].

II. Fabrication Details

A. CNT Forest Growth

Vertically aligned CNT forests from heights of a few micrometers up to nearly 1 mm were synthesized by atmospheric-pressure CVD in a 1-in quartz tube furnace (Lindberg Blue M EW-33850), from a catalyst film patterned using liftoff (AZ3330 photoresist lifted off with Microposit 1165). The substrate and catalyst film consist of 4 nm of patterned Fe (thermally evaporated below 4 μtorr) on 20 nm of unpatterned Al_2O_3 (electron beam evaporated below 30 μtorr) and on a substrate. We have grown VACNTs on various substrates (Si, SiO_2 on Si, Si_3N_4 on Si, and bulk tungsten), with no observable effect on forest growth. Using nonsilicon substrates may enable future niche applications, for example, in temperature-resistant MEMS for use at temperatures above the melting point of the usual Si substrate. The samples are heated from room temperature to 750 °C in about 8 min while flowing 500 sccm of H_2, and then, 700 sccm of C_2H_4 is added. This results in an initial growth rate of about 1 μm/s; however, the growth rate may be tuned by introducing a carrier gas such as Ar and tuning the ratio of gases [16]. The sample is then cooled to below 200 °C in Ar in about 5 min and removed from the furnace.

B. CNT Forest Filling

The forests were filled with a conformal polycrystalline Si film by LPCVD (Canary stack furnace) at 200 mtorr and 580 °C while flowing 20 sccm of SiH_4, for 2 h and 50 min, resulting in a deposition rate on a planar surface (or, equivalently, a radial deposition rate on CNTs) of 1.8 nm/min. For the silicon nitride-filled forests, the nitride was deposited at 720 °C and 200 mtorr (using a different tube) while flowing dichlorosilane (10 sccm) and ammonia (14 sccm) for 3 h. The refractive index of a silicon nitride film of known thickness on a planar Si surface was 1.9, revealing the nitride to be nearly stoichiometric Si_3N_4 (stoichiometric index $= 2.0$). For demonstration purposes, some forests were also filled with a thin layer of Si before filling with Si_3N_4. This bilayer technique may be useful for protecting the CNT framework if the deposition conditions of a particular filler tend to etch the nanotubes.

C. Release

We removed the thin "floor layer" by RIE (Anelva DEM-451) at 100 W and 100 mtorr while flowing O_2 (3.1 sccm) and CF_4 (25 sccm) for 5–9 min, which also removed some of the nanocomposite material from the top of the filled forests. The device itself was preserved because it consisted of features that were much larger than the thickness of the floor layer. The underlying 3-μm PECVD-deposited SiO_2 sacrificial layer was removed by immersion in buffered oxide etch (BOE), and the sample was rinsed in deionized water and was dried.

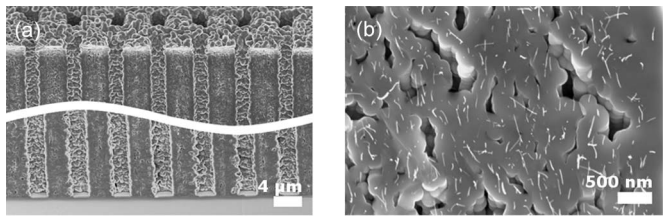

Fig. 3. Nanotube forest filling. (a) Top and bottom of a Si-filled forest, which is 170 μm tall, grown in the same grid pattern shown in Fig. 1(a). The sample has been cleaved open, showing excellent filling uniformity throughout the forest. (Without the vapor access holes shown, only the top 20 μm or so fills solidly.) The holes have become slightly smaller at the top due to the silicon that coats the nanotubes more thickly there. If these vapor access holes are designed to be much smaller than the holes in the moving parts of the MEMS device, the floor layer at the bottom of these holes is not removed in the RIE step, and these regions can serve as anchors to the substrate. Both images were taken at 50° tilt from the plane of the substrate. (b) Filled forest of nanotubes was cleaved in a plane running almost parallel to the tube direction and imaged by SEM. Nanotubes are visibly protruding from the nanocomposite. Voids formed during filling are also visible and comprise about 7% of the volume. Imaged at 50° tilt from the direction that is normal to the cleave plane.

III. Design Considerations

CNT forests can be grown to be several millimeters tall [17], [18], but because long nanotubes are not rigid and the forest has such a low density, small features like pillars or thin lines will bend over if grown too tall [Fig. 1(c)]. Such nonvertical growth is undesirable in most applications. Accordingly, nanotube forests must either be grown short enough, such that the narrowest features do not bend over, or the narrowest features must be redesigned. We have developed self-supporting architectures, such as the crossbar design shown in Fig. 1(c) and (d), which allow forests patterned in lines to be grown to much higher aspect ratios while still remaining thin and are hence highly compliant if they are released as part of a microstructure. Periodic "crossbars," such as those shown in Fig. 1(c) that are 3 μm wide, 10 μm long, and spaced 25 μm apart, allow a 5-μm-wide wall to be grown taller than 100 μm without bending (Fig. 1(c), left). In contrast, the same width wall without supporting crossbars begins to bend significantly if grown above 25 μm tall (Fig. 1(c), right).

Apart from small voids, as discussed in Section V-B, small patterned features (less than a few tens of micrometers wide) are filled completely, and large features are filled sufficiently, such that they are sealed on the outer (side and top) walls, to a depth of a few tens of micrometers. The base of the features is sealed by a thin "internal" floor layer. In principle, the inner regions of the large features have a sufficient density of interconnected voids to be permeable by the BOE used to release the structure; however, even after a short RIE to remove the floor layer, the liquid-permeable interior regions are still well sealed from BOE or other liquids by the solid outer (side, top, and bottom) walls of the large features.

If it is required to fill very tall and wide devices completely (without extensive regions of interconnected voids at the center of the large feature), vapor access holes like those shown in Fig. 3(a) are required in order for the LPCVD precursor gas to penetrate deep inside the forest. Without these holes, only the top 20 μm or so of the forest is solidly filled. However if

3-μm-diameter vapor access holes are added to large parts of the structure in the original lithographic pattern, forests of up to 200 μm tall can completely be filled from top to bottom, and this infiltration depth can likely be improved more by optimization of filling conditions. We have grown even taller structures, up to 1 mm tall, which require larger vapor access holes for complete forest infiltration. If the vapor access holes are made much smaller than the areas where the floor layer is to be removed, then the RIE floor layer removal step does not significantly etch the floor layer at the bottom of the vapor access holes. This is useful for anchoring large thick pads to the substrate while still having them well filled with the filler material.

IV. Methods

A. Electrical Characterization

We measured the sheet resistance of silicon-, silicon nitride-, and bilayer (silicon followed by silicon nitride)-filled forests using a collinear four-point probe measurement device (Magnetron Instruments 750-1) on lithographically patterned 0.5 cm $\times$ 0.5 cm forests of various heights. The raw measurements were then corrected for the sample-probe geometry using the tables in [19].

B. Mechanical Characterization

To test the mechanical properties of the nanocomposite, silicon-filled VACNT cantilevers of various dimensions were fabricated and bent in-plane (perpendicular to the direction of the nanotubes) using a flexible steel wire with a Young's modulus of 200 ± 10 GPa. The testing configuration is shown in Fig. 4(b). The length of steel wire was adjusted until the spring constant of the wire was approximately equal to the spring constant of the cantilever, so that when the steel actuator was used to bend the nanocomposite cantilever, they both deflected measurably under a microscope. The steel actuator and nanocomposite cantilever were touched at the tips, and the steel actuator was moved using a micrometer while the nanocomposite cantilever was held fixed. That is to say, if the micrometer (and, therefore, the attached steel actuator) was moved a distance u_a and the distance that the common point at the tips of the two beams moved was observed to move a distance u (which is less than u_a), then the displacement of the tip of the nanocomposite cantilever was u and the displacement of the tip of the steel actuator relative to its clamped point was $u_a - u$. Distance measurements on the micrometer and the optical microscope were calibrated by comparing them to a commercial $x-y$ calibration standard.

Knowing the dimensions and Young's modulus of the steel actuator, the Young's modulus of the nanocomposite cantilever may be extracted. For small deflections, the Young's modulus of the nanocomposite cantilever E is related to the Young's modulus of the steel actuator E_a by

$$E = E_a \frac{I_a}{I} \frac{u_a}{u} \frac{L^3}{L_a^3} \tag{1}$$

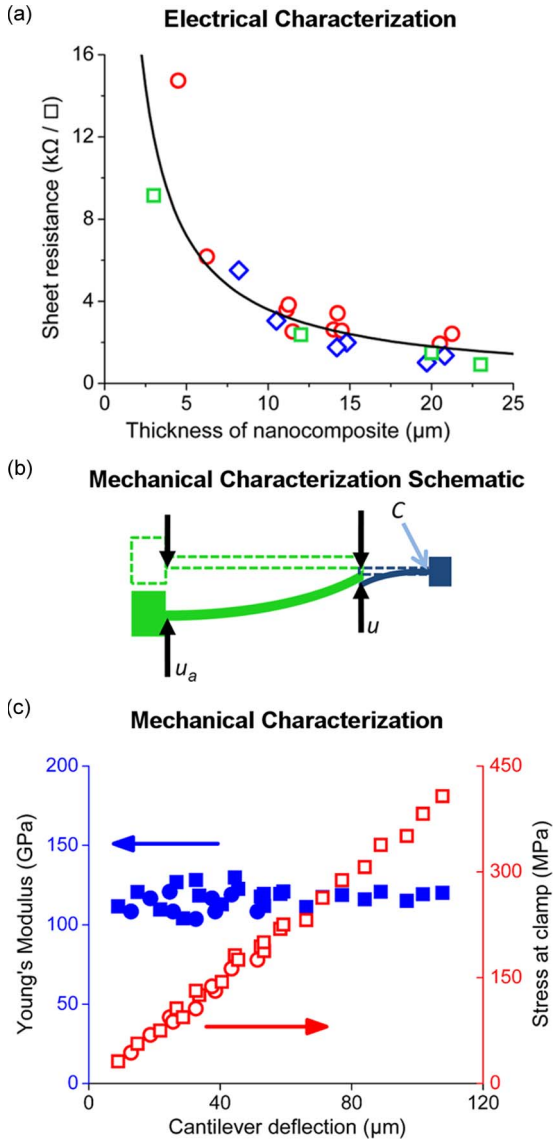

Fig. 4. Electrical and mechanical properties. (a) Sheet resistance versus thickness for (red circles) silicon-filled forests, (green squares) silicon nitride-filled forests, and (blue diamonds) 20 nm of silicon followed by filling with silicon nitride reveals the expected inverse proportionality relationship. The solid line is calculated for a model sample with a resistivity of 3.6 $\Omega \cdot$ cm. (b) Diagram indicating the testing configuration for measuring displacement u at the common point of (light green) the steel actuator and (dark blue) the nanocomposite cantilever in (dotted lines) the unstressed configuration and (solid figure) after the steel actuator has been moved a distance u_a. The distances u and u_a refer to the distances between opposing arrows and were measured in an optical microscope. Point C is the point of maximal stress in the nanocomposite cantilever. (c) (Blue solid data) Young's modulus and (red open data) stress at the clamped point C for Si-CNT cantilevers are calculated from u. Two different cantilevers of identical dimensions are represented here as circles and squares, respectively. The Young's modulus is approximately 120 GPa. The calculated Young's modulus is approximately constant, and the calculated stress at point C follows the expected linear relationship for small deflections.

where I is the second moment of inertia, u is the deflection at the tip, and L is the length for the nanocomposite cantilever (no subscript) and the steel actuator (with subscript a).

To model the effect of the presence of nanotubes on the Young's modulus of the composite, we begin by assuming that the composite consists of a matrix (Young's modulus E_m) containing a volume fraction f of aligned continuous fibers

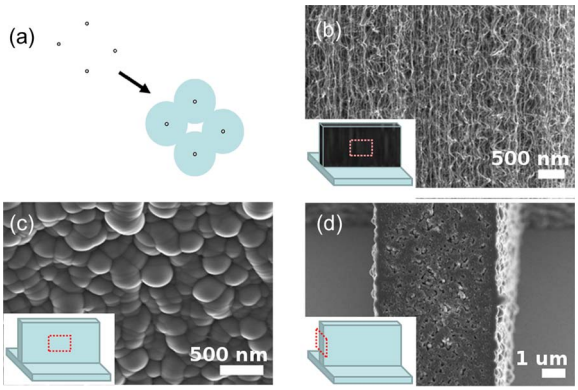

Fig. 5. Nanotube filling and void formation. (a) Four nanotubes are shown schematically in cross section. The tubes are radially coated by the filler material, leaving some voids in the composite. (b) SEM image showing the outside of an as-grown forest. The dotted red box in the inset indicates schematically the location of the image on a wall of nanotubes. (c) Outer wall of the forest after filling with silicon. The inset shows the location of the image. (d) Cleaved cross section of a silicon-filled forest. The dotted box in the inset indicates the location of this image. These SEM images were all taken at 50° tilt.

(Young's modulus E_n). The Halpin–Tsai equation [20] gives the Young's modulus of the composite as

$$E_\perp = E_m \frac{1+\xi\eta f}{1-\eta f} \tag{2}$$

where

$$\eta = \frac{\left(\frac{E_n}{E_m}-1\right)}{\left(\frac{E_n}{E_m}+\xi\right)}. \tag{3}$$

Here, ξ may be taken as an adjustable parameter but is generally on the order of unity (we will take $\xi = 1$).

However, the nanotubes are not straight and parallel but are wavy [Fig. 5(b)] and have a significant component of their length in the direction parallel to the substrate, so it may also be instructive to examine Young's modulus parallel to the nanotube direction ($E_\parallel$). By the "rule of mixtures" [20]

$$E_\parallel = (1-f)E_m + fE_n. \tag{4}$$

V. Results

A. Electrical Characterization

We found the sheet resistance to be inversely proportional to the sample thickness [Fig. 4(a)], indicating that conductivity is proportional to thickness, as expected for samples that are much thinner than the probe spacing. These measurements of sheet resistance in a horizontal direction (perpendicular to the direction of tube growth) appear to be unaffected by whether the filler is silicon, silicon nitride, or a silicon nitride–silicon bilayer. From these measurements, the resistivity was found to be 3.6 $\Omega \cdot$ cm (standard deviation of 1.1 $\Omega \cdot$ cm). It is notable that the resistivity of the nanocomposite is six orders of magnitude lower than the resistivity of undoped polysilicon and 14 orders of magnitude lower than the resistivity of silicon nitride, demonstrating that the vertically oriented nanotubes provide a horizontal conducting path through the composite.

B. Mechanical Characterization

Data from two identical Si-CNT singly clamped cantilevers of dimensions 21 μm $\times$ 37 μm $\times$ 1000 μm are shown in Fig. 4(b). The nanocomposite cantilevers had a Young's modulus of approximately $E_\perp = 120$ GPa, where the subscript refers to the fact that the cantilever was bent in-plane, which is a direction perpendicular to the orientation of the nanotubes.

This value is slightly lower than that of bulk polysilicon (140–210 GPa, highly dependent on deposition conditions [21]) probably partly due to voids in the nanocomposite (Figs. 3(b) and 5). These voids are formed during LPCVD deposition because tubes are coated radially with the filler material and some small regions naturally become shut off from further deposition [Fig. 5(a)].

SEM image analysis on the cleaved cross section of the Si-CNT nanocomposite shown in Fig. 3(b) reveals that silicon comprises over 99% of the mass and about 93% of the volume of the composite (including voids—the Si volume fraction excluding the voids is over 99%). The remainder comprises CNTs (separated by an average inter-tube spacing of about 600 nm) and voids.

As a first approximation, we assume that the composite consists of straight nanotubes embedded in silicon with all voids filled in with the filler material, and therefore, we use (2) with $f = 0.01$, $E_m = 170$ GPa for polysilicon [21], and $E_n = 1000$ GPa [22]. We find that $E_\perp \approx E_m$ to within about 1%. In this model, the nanotubes do not contribute significantly to Young's modulus.

However, as mentioned in Section IV, the nanotubes are not straight and parallel but wavy. Therefore, there is a component of the nanotubes that is running in a direction parallel to the direction of induced stress in our cantilever-testing experiments. As a rough estimate, the Young's modulus of this model may therefore be considered to lie somewhere between the two extreme cases described by (2) and (4). Using (4) with the same f, E_m, and E_n, we find that $E_\parallel$ is still only 5% bigger than E_m. Evidently, the nanotube volume fraction is so small such that the nanotubes do not contribute significantly to the Young's modulus of the composite despite the large Young's modulus of individual nanotubes. Thus, the filler material may be relied on in many cases to provide the mechanical properties, while the framework acts primarily as a passive framework for building MEMS out of the filler material.

Next, we consider the effect of the voids on Young's modulus. A cross-sectional area has about 7% areal density of voids, modifying the second moment of inertia (I) in (1) from that of a solid polysilicon cantilever. The second moment of inertia depends on the size, shape, and location of the individual voids in each cross section, and these are unknown quantities. Therefore, we do not estimate their effect on I, although it is clear that the presence of voids will decrease I, thereby decreasing E from its bulk value. Consequently, our estimation of $E = 120$ GPa should be taken as a conservative lower bound for the composite's Young's modulus. Other nanoscale effects

such as stress concentration around voids and nanotubes may also contribute, decreasing E from that of bulk polysilicon.

C. Devices Fabricated

We demonstrated the processability of these nanocomposite structures by fabricating high-aspect-ratio MEMS that are electrically conductive, even when filled with an insulator such as silicon nitride. The devices that we fabricated included comb drives, cantilevers, bistable mechanisms (BSMs), and thermomechanical in-plane microactuators (TIMs). Unlike [7], we do not observe any curl-up of cantilevers after release for silicon- or silicon nitride-infiltrated cantilevers, even for our lowest aspect-ratio cantilevers (i.e., short forest growth compared to the width of the cantilever). Silicon-infiltrated comb drives are presented in [1].

Prototype silicon nitride-infiltrated BSMs that may be useful as microswitches requiring two well-defined positions [23] or as accelerometers [24] are shown in Fig. 6(a)–(c).

We also fabricated silicon-filled TIMs, as shown in Fig. 6(d) and (e). When a current is passed through its narrow legs, the legs thermally expand and push the central shuttle piece forward [25]. We achieved a displacement of 10 μm for our devices at a voltage of 160 V, after which the devices could not support larger currents and broke, forming an open circuit.

High aspect ratios are desirable in comb drives, BSMs, and TIMs in order to increase available force output and robustness and decrease out-of-plane motion. It is envisaged that this technique may be used to fabricate MEMS using filler materials that can withstand high temperatures or harsh chemical environments or to provide greater transducing capability (such as TIMs filled with a material with high thermal expansion coefficient).

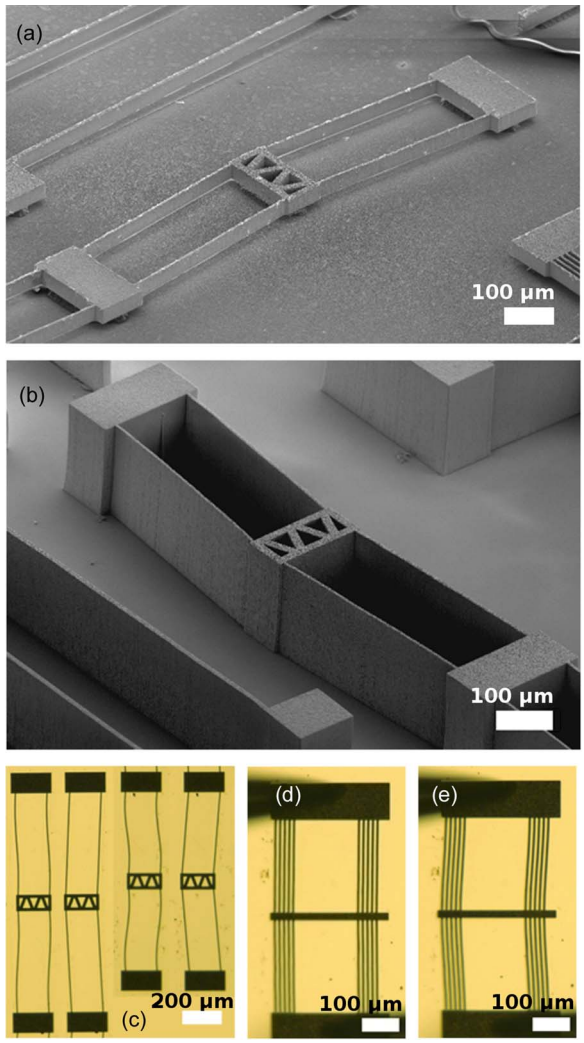

Fig. 6. MEMS devices fabricated using the CNT framework technique. (a) SEM image of a released working BSM made from a silicon nitride-CNT nanocomposite. (b) SEM image of an unreleased silicon nitride–CNT composite, demonstrating the remarkably large aspect ratios that are achievable. The narrower features on this device are well filled, but the larger pads have substantial voids in the center. As a result, this particular device did not successfully release. To overcome this problem, as shown in Fig. 3(a) and (b), small 1–3-μm-diameter vapor access holes must be designed in the anchor pads. (c) Composite optical microscope images of Si-CNT nanocomposite BSMs in both configurations, for two different-size devices. (d) Optical microscope images of a TIM in the OFF state (0 V). (e) TIM in the ON state (160 V), showing 10 μm of displacement.

VI. Conclusion

In conclusion, we have exploited nanostructured CNT composites to make mechanically robust high-aspect-ratio structures and various functional MEMS devices. We have developed self-supporting architectures to increase the aspect ratio of the CNT framework for highly compliant flexures. The penetration depth of the filler for very tall structures has been improved by designing vapor access holes that are large enough for the LPCVD precursor to penetrate but too small for RIE removal of the floor layer, allowing large anchor regions to be filled while remaining anchored to the substrate after the release step. We found that Young's modulus for the silicon-filled CNT framework is nearly as high as the value for the polysilicon filler, but the electrical resistivity of the filled CNT framework is approximately 3.6 $\Omega \cdot$ cm, much lower than that of the filler material, and is remarkably similar for both the silicon- and silicon nitride-filled forests. The versatility of the CVD filling step suggests that this technique might be used to make microstructures from a variety of new materials.

Acknowledgment

D. N. Hutchison, N. B. Morrill, and B. W. Turner would like to thank Brigham Young University for the undergraduate mentoring programs. Devices were made in the Brigham Young University Integrated Microelectronics Laboratory and the University of Utah Microfabrication Laboratory and were tested in the Brigham Young University Compliant Mechanisms Research Laboratory.

References

[1] D. N. Hutchison, Q. Aten, B. W. Turner, N. B. Morrill, L. L. Howell, B. D. Jensen, R. C. Davis, and R. R. Vanfleet, "High aspect ratio microelectromechanical systems: A versatile approach using carbon nanotubes as a framework," in *Proc. 15th Int. Conf. Solid-State Sens., Actuators, Microsyst. Transducers*, 2009, pp. 1604–1607.

[2] S. W. Pang, "High aspect ratio structures for MEMS," *Mater. Res. Soc. Bull.*, vol. 26, pp. 307–308, 2001.

[3] J. R. Creighton and P. Ho, "Introduction to chemical vapor deposition (CVD)," in *Chemical Vapor Deposition*, J. H. Park and T. S. Sudarsham, Eds. Materials Park, OH: ASM, 2001, p. 2.

[4] D. N. Futaba, K. Hata, T. Yamada, T. Hiraoka, Y. Hayamizu, Y. Kakudate, O. Tanaike, H. Hatori, M. Yumura, and S. Iijima, "Shape-engineerable and highly densely packed single-walled carbon nanotubes and their application as super-capacitor electrodes," *Nat. Mater.*, vol. 5, no. 12, pp. 987–994, Nov. 2006.
[5] Y. Hayamizu, T. Yamada, K. Mizuno, R. C. Davis, D. N. Futaba, M. Yumura, and K. Hata, "Integrated three-dimensional microelectromechanical devices from processable carbon nanotube wafers," *Nat. Nanotechnol.*, vol. 3, no. 5, pp. 289–294, May 2008.
[6] L. Ci, J. Suhr, V. Pushparaj, X. Zhang, and P. M. Ajayan, "Continuous carbon nanotube reinforced composites," *Nano Lett.*, vol. 8, no. 9, pp. 2762–2766, 2008.
[7] W. Fang, H.-Y. Chu, W.-K. Hsu, T.-W. Cheng, and N.-H. Tai, "Polymer-reinforced, aligned multiwalled carbon nanotube composites for microelectromechanical systems applications," *Adv. Mater.*, vol. 17, no. 24, pp. 2987–2992, 2005.
[8] W.-K. Hsu, H.-Y. Chu, T.-H. Chen, T.-W. Cheng, and W. Fang, "An exceptional bimorph effect and a low quality factor from carbon nanotube–polymer composites," *Nanotechnology*, vol. 19, no. 13, p. 135 304, Feb. 2008.
[9] B. L. Wardle, D. S. Saito, E. J. Garcia, A. J. Hart, R. G. de Villoria, and E. A. Verploegen, "Fabrication and characterization of ultrahigh-volume-fraction aligned carbon nanotube–polymer composites," *Adv. Mater.*, vol. 20, no. 14, pp. 2707–2714, 2008.
[10] E. H. T. Teo, W. K. P. Yung, D. H. C. Chua, and B. K. Tay, "A carbon nanomattress: A new nanosystem with intrinsic, tunable, damping properties," *Adv. Mater.*, vol. 19, no. 19, pp. 2941–2945, 2007.
[11] Q. Ngo, B. A. Cruden, A. M. Cassell, G. Sims, M. Meyyappan, J. Li, and C. Y. Yang, "Thermal interface properties of Cu-filled vertically aligned carbon nanofiber arrays," *Nano Lett.*, vol. 4, no. 12, pp. 2403–2407, Dec. 2004.
[12] J. Li, R. Stevens, L. Delzeit, H. T. Ng, A. Cassell, J. Han, and M. Meyyappan, "Electronic properties of multiwalled carbon nanotubes in an embedded vertical array," *Appl. Phys. Lett.*, vol. 81, no. 5, pp. 910–912, 2002.
[13] A. Chandrashekar, S. Ramachandran, G. Pollack, J.-S. Lee, G. S. Lee, and L. Overzet, "Forming carbon nanotube composites by directly coating forests with inorganic materials using low pressure chemical vapor deposition," *Thin Solid Films*, vol. 517, no. 2, pp. 525–530, Nov. 2008.
[14] Y. Hayamizu, R. C. Davis, T. Yamada, D. N. Futaba, S. Yasuda, M. Yumura, and K. Hata, "Mechanical properties of beams from self-assembled closely packed and aligned single-walled carbon nanotubes," *Phys. Rev. Lett.*, vol. 102, no. 17, p. 175 505, May 2009.
[15] C. K. Malek and V. Saile, "Applications of LIGA technology to precision manufacturing of high-aspect-ratio micro-components and -systems: A review," *Microelectron. J.*, vol. 35, no. 2, pp. 131–143, Feb. 2004.
[16] S. P. Patolea, P. S. Alegaonkarb, H.-C. Leeb, and J.-B. Yoo, "Optimization of water assisted chemical vapor deposition parameters for super growth of carbon nanotube," *Carbon*, vol. 46, no. 14, pp. 1987–1993, Nov. 2008.
[17] S. Chakrabarti, T. Nagasaka, Y. Yoshikawa, L. Pan, and Y. Nakayama, "Growth of super long aligned brush-like carbon nanotubes," *Jpn. J. Appl. Phys.*, vol. 45, no. 24–28, pp. L720–L722, 2006.
[18] X. Li, X. Zhang, L. Ci, R. Shah, C. Wolfe, S. Kar, S. Talapatra, and P. M. Ajayan, "Air-assisted growth of ultra-long carbon nanotube bundles," *Nanotechnology*, vol. 19, no. 45, p. 455 609, Oct. 2008.
[19] F. M. Smits, "Measurements of sheet resistivities with the four-point probe," *Bell Syst. Tech. J.*, vol. 37, pp. 711–718, 1958.
[20] D. Hull, *An Introduction to Composite Materials*. New York: Cambridge Univ. Press, 1981.
[21] L. Elbrecht and J. Binder, "The mechanical properties of thin polycrystalline silicon films as function of deposition and doping conditions," *Sens. Mater.*, vol. 11, no. 3, pp. 163–179, 1999.
[22] M. Meyyappan, Ed., *Carbon Nanotubes*. Boca Raton, FL: CRC Press, 1996, p. 74.
[23] B. D. Jensen and L. L. Howell, "Bistable configurations of compliant mechanisms modeled using four links and translational joints," *J. Mech. Des.*, vol. 126, no. 4, pp. 657–666, Jul. 2004.
[24] B. J. Hansen, C. J. Carron, B. D. Jensen, A. R. Hawkins, and S. M. Schultz, "Plastic latching accelerometer based on bistable compliant mechanisms," *Smart Mater. Struct.*, vol. 16, no. 5, pp. 1967–1972, Sep. 2007.
[25] C. D. Lott, T. W. McLain, J. N. Harb, and L. L. Howell, "Modeling the thermal behavior of a surface-micromachined linear-displacement thermomechanical microactuator," *Sens. Actuators A, Phys.*, vol. 101, no. 1/2, pp. 239–250, Sep. 2002.

David N. Hutchison was born and raised in Auckland, New Zealand. He received the B.S. degree (*magna cum laude*) in physics from Brigham Young University, Provo, UT, in 2008. He is currently working toward the Ph.D. degree in the School of Applied and Engineering Physics, Cornell University, Ithaca, NY, working with Dr. Sunil Bhave.

His research interests at Cornell include graphene device physics and micro-opto-electromechanical systems.

Mr. Hutchison was the recipient of a Lester B. Knight Fellowship in 2008 and a Cornell Nanofabrication Facility Fellowship in 2009.

Nicholas B. Morrill was born in Mission Viejo, CA, in 1986. He is currently working toward the B.S. degree in physics in the Department of Physics and Astronomy, Brigham Young University, Provo, UT.

He was recently a Student Trainee Engineer with the Goddard Space Flight Center, National Aeronautics and Space Administration.

Mr. Morrill is a member of the American Physical Society.

Quentin Aten received the B.S. and M.S. degrees in mechanical engineering from Brigham Young University, Provo, UT, in 2007 and 2008, respectively, where he is currently working toward the Ph.D. degree in the Department of Mechanical Engineering.

During his undergraduate studies, he contributed to the feedback control of piezoresistively controlled microelectromechanical systems (MEMS) thermal actuators. His graduate research focuses on compliant MEMS mechanisms, with specific application to bio-MEMS devices for genetically transforming living cells.

Brendan W. Turner received the B.S degree in physics from Brigham Young University (BYU), Provo, UT, in 2008. He is currently working toward the Ph.D. degree in Applied Science and Technology at the University of California at Berkeley.

At BYU, his research focused on the patterned growth of vertically aligned carbon nanotubes and their application as device scaffolds. His graduate research focuses on nanoplasmonic substrates for optical detection of biomolecules.

Brian D. Jensen received the B.S. and M.S. degrees in mechanical engineering from Brigham Young University (BYU), Provo, UT, in 1996 and 1998, respectively, and the M.S. degree in electrical engineering and the Ph.D. degree in mechanical engineering from the University of Michigan, Ann Arbor, both in 2004.

In 1998 and 1999, he spent 16 months as a Micromechanism Designer at Sandia National Laboratories, Albuquerque, NM. He has served as an Assistant Professor in the Mechanical Engineering Department at BYU since January 2005. He has performed research and published over 60 papers in design topics, including microelectromechanical systems and compliant mechanisms, and he is a holder of seven U.S. patents. He was also the recipient of a National Science Foundation Graduate Research Fellowship and a Department of Defense Science and Engineering Graduate Fellowship.

Larry L. Howell received the B.S. degree from Brigham Young University (BYU), Provo, UT, in 1987, and the M.S. and Ph.D. degrees from Purdue University, West Lafayette, IN, in 1991 and 1993, respectively.

He is a Professor and the Past Chair of the Department of Mechanical Engineering, BYU, where he currently holds a University Professorship. Prior to joining BYU in 1994, he was a Visiting Professor at Purdue University, West Lafayette, IN, a Finite-Element Analysis Consultant for Engineering Methods, Inc., and an Engineer working on the design of the YF-22 (the prototype for the U.S. Air Force F-22). His patents and technical publications focus on compliant mechanisms and microelectromechanical systems. He is the author of the book *Compliant Mechanisms* (Wiley, 2001).

Dr. Howell is a Fellow of the American Society of Mechanical Engineers (ASME), the Past Chair of the ASME Mechanisms and Robotics Committee, and an Associate Editor for the *Journal of Mechanical Design*. He is the recipient of an ASME Mechanisms and Robotics Award, an NSF CAREER Award, an ASME Design Automation Conference Best Paper Award, a BYU Technology Transfer Award, and a Maeser Research Award.

Richard R. Vanfleet received the B.S. degree in physics from Brigham Young University (BYU), Provo, UT, in 1992, and the M.S. and Ph.D. degrees in physics from the University of Illinois, Urbana, in 1994 and 1997, respectively.

From 1997 to 1999, he was a Postdoctoral Researcher in the School of Applied and Engineering Physics, Cornell University, Ithaca, NY. From 1999 to 2003, he was a member of the Faculty at the University of Central Florida (UCF), Orlando. At UCF, he held a joint appointment in the Department of Physics and the Advanced Materials Processing and Analysis Center. He has been with the Department of Physics and Astronomy, BYU, since September 2003.

Robert C. Davis received the B.S. degree in physics from Brigham Young University (BYU), Provo, UT, in 1989, and the Ph.D. degree from the University of Utah, Salt Lake City, in 1996.

He was a Postdoctoral Researcher at Cornell University, Ithaca, NY, from 1996 to 1998, and a Visiting Researcher at the National Institute of Advanced Industrial Science and Technology, Tsukuba, Japan, in 2006 and 2007. He joined the Brigham Young University Department of Physics and Astronomy in 1998 where he is presently an Associate Professor. He is also a member of the Center for Nanoscale Systems, Cornell University. His research in micro- and nanofabrication, chemical surface patterning, microscopy, and analysis has resulted in 35 publications and 11 patents.